Bulletin of the JSME Vol.20, No.1, 2025
Journal of Biomechanical Science and Engineering

Helical swimming motion driven by coordinated rotation of flagellar apparatus in marine bacterial cells

Yuji SHIMOGONYA*, Juanfang RUAN**, Takayuki KATO***, Takuji ISHIKAWA****,†, Keiichi NAMBA**,††, Long-Fei WU††† and Masayoshi NISHIYAMA††††

* Department of Mechanical Engineering, College of Engineering, Nihon University
1 Nakagawara, Tokusada, Tamuramachi, Koriyama, Fukushima 963-8642, Japan
E-mail: shimogonya.yuji@nihon-u.ac.jp
** Graduate School of Frontier Biosciences, Osaka University
1-3 Yamadaoka, Suita, Osaka 565-0871, Japan
*** Institute for Protein Research, Osaka University
1-3 Yamadaoka, Suita, Osaka 565-0871, Japan
**** Department of Biomedical Engineering, Graduate School of Biomedical Engineering, Tohoku University
6-6-01 Aoba, Sendai, Miyagi 980-8579, Japan
† Department of Finemechanics, Graduate School of Engineering, Tohoku University
6-6-01 Aoba, Sendai, Miyagi 980-8579, Japan
†† JEOL YOKOGUSHI Research Alliance Laboratories, Osaka University
1-3 Yamadaoka, Suita, Osaka 565-0871, Japan
††† Aix Marseille Université, CNRS, Laboratoire de Chimie Bactérienne
F-13402 Marseille Cedex 20, France
†††† Department of Science, Faculty of Science and Engineering, KINDAI University
3-4-1 Kowakae, Higashiosaka, Osaka 577-8502, Japan

Received: 29 July 2024; Revised: 15 September 2024; Accepted: 8 October 2024

Abstract

The magnetotactic bacterium MO-1 possesses a pair of unique flagellar apparatuses. Each apparatus comprises seven flagella and 24 thin fibrils enclosed in a sheath. Using these apparatuses, the cells swim at high speed through solutions, tracing helical trajectories. The mechanism by which MO-1 cells utilize their two flagellar apparatuses to propel the cell body remains unclear. Due to the short length of the flagellar apparatus, direct observation of individual movements under a microscope is technically challenging. In this study, we performed numerical simulations based on the boundary element method to investigate the swimming motility of MO-1 cells. Our cell models successfully reproduced the helical trajectories of active MO-1 cells. The two flagellar apparatuses were positioned at the front and back of the cell body relative to the direction of movement. The cell body was pulled by the anterior flagellar apparatus and pushed by the posterior apparatus. The swimming motion of the cell model exhibited minimal changes near a wall. This unique swimming behavior of MO-1 cells could only be achieved through the rotation of both flagellar apparatuses. Based on the revolution rate of active MO-1 cells, we estimated the rotational speed of the flagellar apparatus to be approximately 1200 s^{-1}. This rapid rotation may result from the tight packing of flagellar filaments within the sheath. Our study elucidates the mechanism by which active MO-1 cells swim in helical trajectories.

Keywords: Bacterium, Flagellum, Swimming, Bacterial motility, Flagellar rotation, Helix chirality, Helical trajectory, Numerical simulation, Boundary element method (BEM)

1. Introduction

Many bacteria possess various motility machineries that enable them to navigate to more favorable environments (Miyata et al., 2019). These machines generate diverse locomotive patterns. Bacterial flagella represent the most typical motility machineries (Berg, 2003; Homma and Kojima, 2022; Minamino and Kinoshita, 2023; Armitage, 2024). An

Paper No.24-00284
J-STAGE Advance Publication date : 18 October, 2024
[DOI: 10.1299/jbse.24-00284]

Escherichia coli (*E. coli*) cell exhibits several helical filaments, each 10 μm in length. A protein-based molecular motor (flagellar motor) connects to the root of the flagellum. The flagellar motor, driven by ion-motive force, generates propulsive force by rotating the attached flagella, thus propelling the bacterium through solution. The trajectories of the cells in solution are straight, but they display curving near surfaces. Their swimming speed reaches several tens of micrometers per second.

Magnetotactic bacteria swim along magnetic field lines (Blakemore, 1975). *Magnetococcus massalia* strain MO-1, hereafter referred to as MO-1, is a magnetotactic bacterial species discovered in the Mediterranean in 2009 (Lefèvre et al., 2009; Ji et al., 2017; Zhang and Wu, 2020). An MO-1 cell displays two bundles of motile organs, one near each pole of the cell body. Each bundle comprises seven flagella encased in a sheath (Lefèvre et al., 2010). Electron cryotomography of the three-dimensional structure within the sheath revealed that 24 thin fibrils surround the seven flagella, with their basal bodies neatly arranged in a hexagonal array (Ruan et al., 2012; Zhang et al., 2012). Using these two flagellar apparatuses, MO-1 cells swim smoothly in solution with a helical trajectory. Their swimming speed exceeds that of *E. coli* by several fold (Zhang et al., 2014). The mechanism through which this unique motion is produced by two flagellar apparatuses remains unknown because the short length of the flagellar apparatus makes it technically challenging to observe movement under a microscope.

Recently, Bente et al. (2020) studied the swimming motility of MC-1, a species closely related to MO-1. They modeled the MC-1 cell body as a single sphere and the flagellar bundle as 20 beads. Their investigation of the relationship between the motion of the two flagellar bundles and the swimming trajectory of an MC-1 cell used Stokesian dynamics simulations. This approach reproduced the characteristic helical swimming trajectory of MC-1 cells only when one flagellar bundle pushed the cell body while the other pulled the cell body. Other combinations resulted in helical trajectories with diameters considerably smaller than those observed experimentally. These findings align with previous work (Yang et al., 2012). Although their simulations provided substantial insight, the reasons why MO-1 cells use such a unique flagellar apparatus and swim in a helical trajectory have remained unknown.

In this study, we performed numerical simulations based on the boundary element method to investigate the swimming motility of MO-1 cells. The boundary element method allows for highly accurate analysis of microorganism swimming (Ishikawa et al., 2007; Shum et al., 2010; Shimogonya et al., 2015; Yang et al., 2019; Kogure et al., 2023), making it suitable for our purpose. We modeled all possible combinations of the motions of the two flagellar apparatuses of an MO-1 cell. Additionally, we observed MO-1 cells and measured the diameters and pitches of their helical trajectories, as well as the translational speeds and revolution rates of the cell bodies. We compared the numerical simulation results with observational data to validate our MO-1 cell model.

2. Materials and methods

2.1 MO-1 cell model

As shown in Fig. 1a, an MO-1 cell possesses two curved flagellar bundles. The flagellar apparatuses extend almost perpendicularly from the cell membrane. There is no hook structure like that seen in *E. coli* flagella (Ruan et al., 2012). Fig. 1b illustrates our simulation model of an MO-1 cell, developed to investigate its swimming behavior. We constructed the model with reference to the image in Fig. 1a. As in our previous studies (Giacché et al., 2010; Shimogonya et al., 2015), we treated the cell body shape as a prolate spheroid. We set its polar and equatorial radii to $a = 1$ and $b = 0.75$ μm, respectively. The flagellar base site of actual MO-1 cells can vary due to inter-individual differences. Because this variation may substantially affect the cell's swimming behavior, we treated the sites of the two flagellar bases as variables θ_1 and θ_2, varying them from 20° to 30° at 5° intervals. In our model, each flagellum had a helical centerline, as described by the helix model of Higdon (1979). The flagellar apparatus measured 2 μm in length and 0.1 μm in diameter (Ruan et al., 2012). We set its helix radius and pitch to 1 and 6 μm, respectively, based on Fig. 1a. The flagellar apparatuses extended perpendicularly from the cell surface. The length of the flagellar apparatus is short, and there is no elastic element at its base. Thus, two flagellar apparatuses cannot be bundled, and can rotate individually. When the two flagellar apparatuses rotate, the phase difference in rotation angles between them can range from 0° to 360°. Because this may also affect the swimming behavior of the MO-1 cell model, we performed simulations for cases with phase differences of 0°, 90°, 180°, and 270°. Since the flagellar apparatuses rotate at a constant speed in our simulations, the phase differences remain constant or periodic during the swimming.

[DOI: 10.1299/jbse.24-00284]

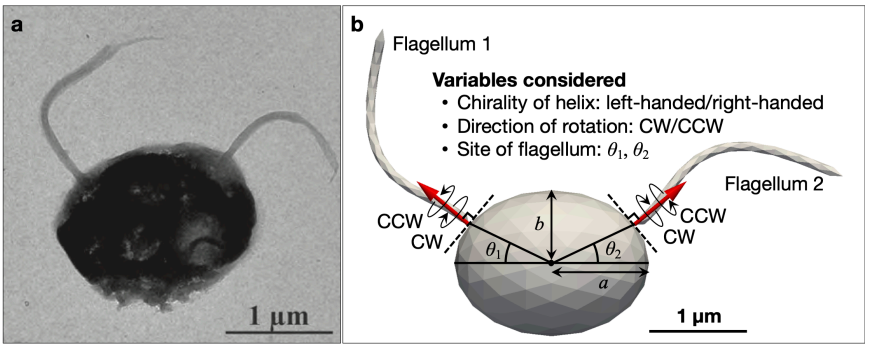

Fig. 1 (a) Negatively stained EM image of an MO-1 cell. (b) Schematic diagram of the computational model of an MO-1 cell. CW, clockwise; CCW, counterclockwise.

2.2 Helix chirality and rotary direction of flagellum

The helix chirality (left- or right-handed) and rotary direction [clockwise (CW) or counterclockwise (CCW)] of an actual MO-1 flagellar apparatus during swimming remain undetermined due to their small size and high swimming speed, which hinder observation. In bacterial swimming, the helix chirality and rotary direction of the flagellar apparatus are key factors that substantially affect swimming behavior. Therefore, we treated the helix chirality and rotary direction of each flagellar apparatus as variables in our numerical simulations. Each flagellar apparatus can have two different helix chiralities (left- or right-handed) and two different rotary directions (CCW or CW), resulting in four possible combinations of flagellar helix chirality and rotational direction. Consequently, all combinations for the two flagellar apparatuses in a cell lead to a total of 16 cases. Table 1 summarizes these combinations and their IDs.

Table 1 Tested combinations of helix chirality and rotary direction of the two flagella and their IDs. L, left-handed; R, right-handed; CW, clockwise; CCW, counterclockwise. The patterns of swimming behavior are also shown.

ID	Flagellum 1		Flagellum 2		Axis of cell body that translational motion is parallel to	Axis of cell body that rotational motion is parallel to
	Chirality of helix	Direction of rotation	Chirality of helix	Direction of rotation		
1	L	CCW	L	CCW	Short axis	Short axis
2	L	CCW	R	CCW	Long axis	Short axis
3	L	CW	R	CCW	Short axis	Long axis
4	L	CW	L	CCW	Long axis	Long axis
5	L	CW	L	CW	Short axis	Short axis
6	L	CW	R	CW	Long axis	Short axis
7	L	CCW	R	CW	Short axis	Long axis
8	L	CCW	L	CW	Long axis	Long axis
9	R	CW	R	CW	Short axis	Short axis
10	R	CW	L	CW	Long axis	Short axis
11	R	CCW	L	CW	Short axis	Long axis
12	R	CCW	R	CW	Long axis	Long axis
13	R	CCW	R	CCW	Short axis	Short axis
14	R	CCW	L	CCW	Long axis	Short axis
15	R	CW	L	CCW	Short axis	Long axis
16	R	CW	R	CCW	Long axis	Long axis

2.3 Basic equations and numerical methods

We numerically simulated the behavior of an MO-1 cell swimming in bulk fluid or near a wall. We assumed that the flagellar apparatuses rigidly rotate in a prescribed direction (CW or CCW) around the axis normal to the cell body (red arrows in Fig. 1b) with a constant rotational speed, $f = 1200$ s^{-1}, relative to the cell body. The rationale and validity of this value will be discussed in Section 3.2 and Chapter 4, respectively. The force-free and torque-free equations govern the swimming motion of the MO-1 cell model (Ishikawa et al., 2007). Due to the small size of a swimming MO-1 cell, the fluid flow around it exists in the Stokes flow regime, allowing the velocity field to be described by the boundary integral equation (Youngren and Acrivos, 1975). We used the boundary element method to discretize the boundary integral equations with the corresponding velocity boundary condition on the model surface (Ishikawa et al., 2007). Using the discretized equations and force-free and torque-free equations, we obtained a system of linear equations that can be solved numerically. We determined the translational speed and revolution rate of the MO-1 cell model by solving the system of linear equations in a manner similar to our previous studies (Ishikawa et al., 2007; Shimogonya et al., 2015).

[DOI: 10.1299/jbse.24-00284]

In our numerical simulations, all physical quantities were nondimensionalized with the cell body polar radius a, the fluid viscosity μ, and the rotational angular velocity of the flagellar apparatus $\omega = 2\pi f$.

2.4 Bacterial strains and experimental procedure

The ovoid magnetotactic strain MO-1 was grown in EMS2 medium at room temperature to exponential phase, as previously described (Lefèvre et al., 2009; Ruan et al., 2012). The culture medium was diluted with EMS-H buffer [330 mM NaCl, 62 mM $MgCl_2$, 23 mM Na_2SO_4, 16 mM $CaCl_2$, 7 mM KCl, 13 mM HEPES buffer (pH 7.2)].

Cell motility was observed by phase-contrast image microscopy (IX71, Olympus, Tokyo, Japan) and recorded at 1000 frames s^{-1} (220 nm per pixel, LRH20000, Digimo, Tokyo, Japan) (Nishiyama and Sowa, 2012; Okuno et al., 2013). All microscopic images were stored in a computer for offline analysis. We selected cells that swam smoothly in the focal plane under the microscope, then constructed a kymograph of the intensity of the phase-contrast images of single cells (Fig. 2a, top). We defined the pitch and diameter of the helical trajectory (Fig. 2a, bottom). We measured the translation speed and revolution rate of the swimming cells by tracking them (Fig. 2b and c).

Cell samples on carbon-coated copper grids were stained with 0.5% (wt/vol) uranyl acetate. The samples were observed and recorded using a JEM-1011 transmission electron microscope operating at 100 kV, equipped with a TVIPS F114 camera.

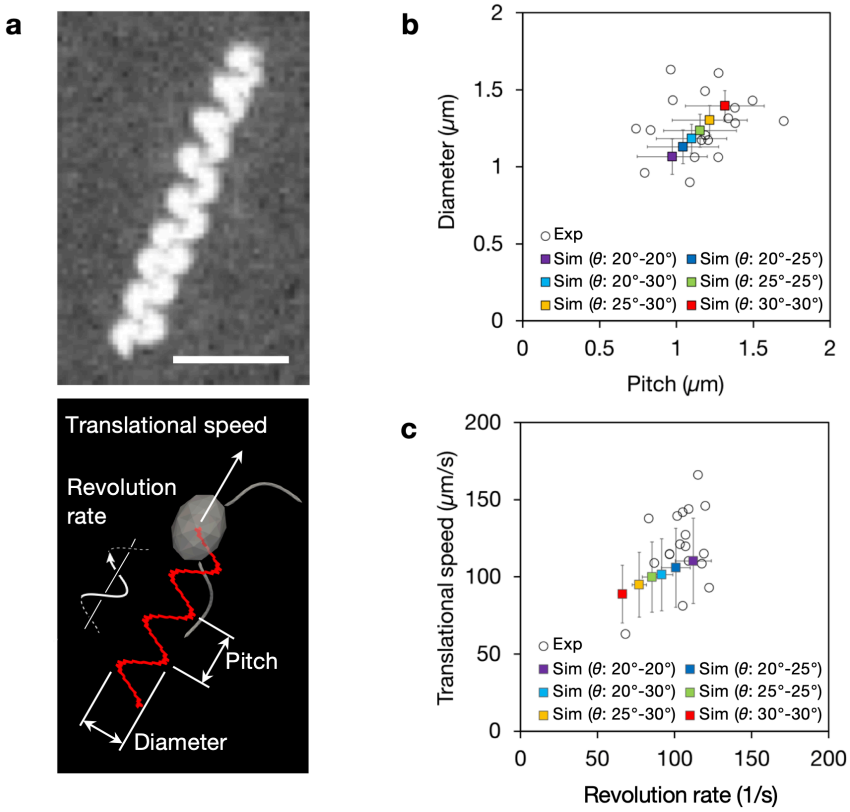

Fig. 2 Comparison of the simulated helical swimming trajectory in ID4 with experimental results. (a) Swimming trajectories of an actual cell (top) and the cell model (bottom). (top) Swimming track of an active cell. We recorded the phase contrast image at a sampling rate of 1000 fps for 100 ms. Scale bar = 5 μm. (bottom) Definitions of the compared quantities. Note: We calculated the translational speed and revolution rate by dividing the direct distance and number of revolutions, respectively, by the elapsed time between two selected points on the swimming trajectory. (b and c) Comparison of simulation and experimental results (*open circles*, n=19). Diameter versus pitch (b) and translational speed versus revolution rate (c). θ is the angle between the long axis of cell body and the line connecting the cell center to each flagellar base (see Fig. 1b). For example, "θ: 20° – 30°" represents $\theta_1 = 20°$ for flagellum 1 and $\theta_2 = 30°$ for flagellum 2. Plots and error bars represent the means and standard deviations of simulation results under four different rotational phase differences (0°, 90°, 180°, and 270°) between the two flagella. All the simulation results are under the assumptions of the cell body polar radius a = 1 μm and the flagellar rotational speed f = 1200 s^{-1}.

[DOI: 10.1299/jbse.24-00284]

3. Results and discussion

3.1 Relationship between flagella motion and swimming trajectory

We performed numerical simulations of the MO-1 cell model swimming in bulk fluid. There are 16 possible combinations of flagellar helix chirality and rotary direction (Table 1). For these simulations, the sites of the two flagellar apparatuses were fixed at $\theta_1 = \theta_2 = 25°$. The rotational phase difference between the two flagellar apparatuses was set at 0°. Figure 3 and Supplementary Video S1 summarize the swimming trajectories of the 16 cases in MO-1 cells.

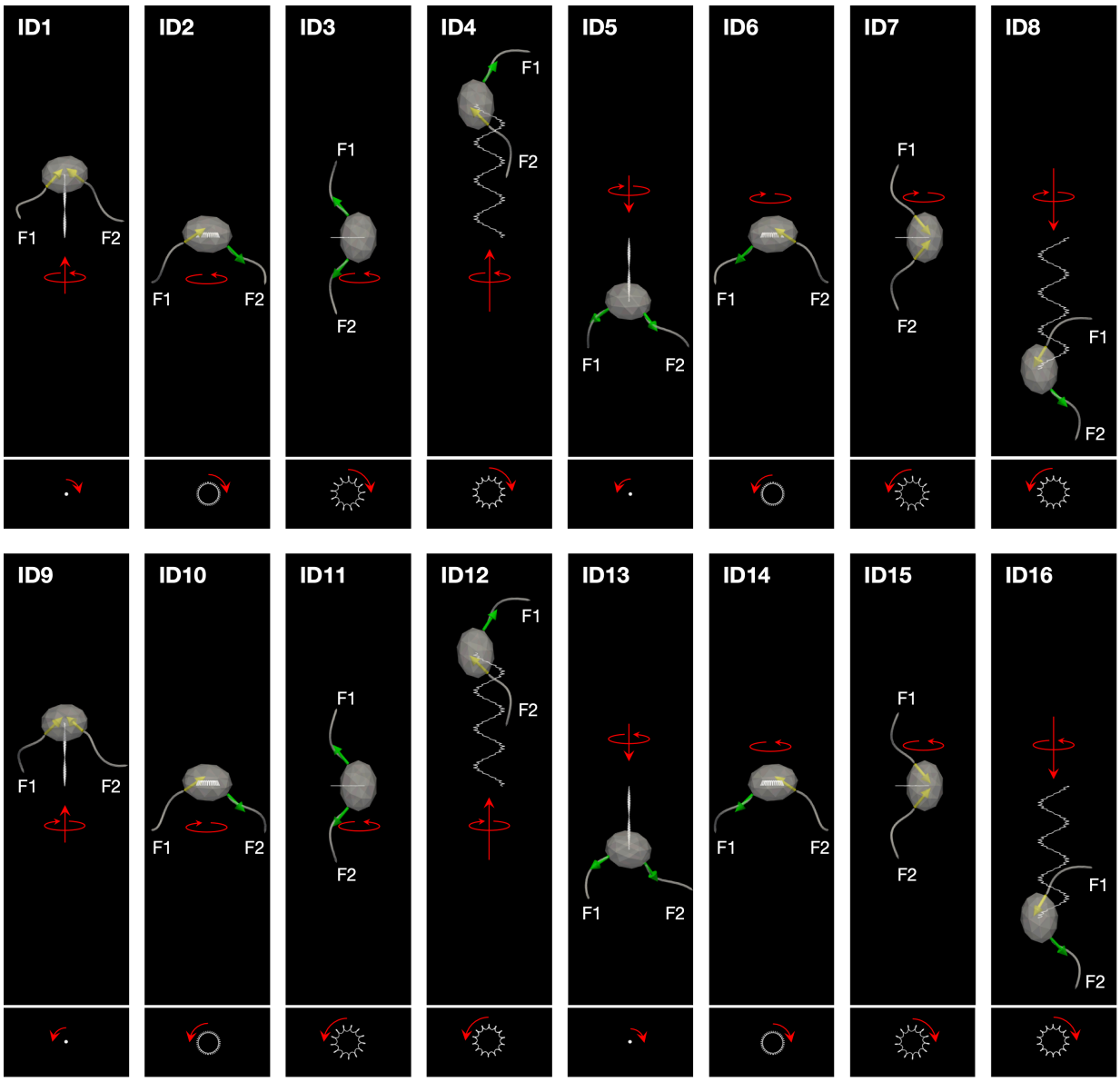

Fig. 3 Front and bottom views of the swimming trajectories of MO-1 cell models with $\theta_1 = \theta_2 = 25°$ for the respective IDs. F1, flagellum 1; F2, flagellum 2; push (yellow); pull (green). The rotational phase difference between the two flagellar apparatuses was set at 0°. For ID4, ID8, ID12, and ID16, the pitch and diameter of the helical trajectory were 1.45 and 1.25 μm, respectively. The ratio of translational speed to revolution rate was 1.48 μm. Although the results for all 16 combinations are shown, there are actually only 8 effective combinations because of the presence of mirror symmetry cases.

The mechanism by which the MO-1 cell model exhibits different swimming trajectories depends on the combination of flagellar helix chirality and rotary direction. The force induced by the flagella on the cell body can be understood as follows. When the flagellar helix is “left-handed” and the rotary direction is “CCW” (when viewed from outside the cell body), the flagellar helical wave travels from the base to the tip of the flagellum. In this situation, the surrounding fluid

[DOI: 10.1299/jbse.24-00284]

experiences a flagellum-induced local force directed away from the cell body. The flagellum, in turn, experiences a reactive local force from the surrounding fluid that causes it to "push" the cell body. Similarly, the combination of "right-handed and CW" results in the flagellum pushing the cell body. Conversely, when the flagellum has the combination "left-handed and CW" or "right-handed and CCW", the flagellum "pulls" the cell body. The MO-1 cell has two flagellar apparatuses; the net force from these apparatuses on the cell body is approximately parallel to either the short (Fig. 4a and b) or long (Fig. 4c and d) axis of the cell body. The net force direction determines the direction of translational motion.

Next, we consider the cell body rotation induced by the flagella. When a flagellar motor torque rotates a flagellum in a certain direction (CW or CCW), the cell body experiences a counter torque from the flagellum. If the rotary directions of the two flagellar apparatuses are either "CCW and CCW" or "CW and CW", the net torque acting on the cell body is approximately parallel to the short axis of the cell body (Fig. 5a and b). Conversely, for "CCW and CW" or "CW and CCW", the net torque is approximately parallel to the long axis of the cell body (Fig. 5c and d). The net torque direction determines the direction of the rotational axis.

Based on the above, we can classify the swimming behavior of the MO-1 cell model into four patterns, according to the combination of translation and rotation directions, as summarized in Table 1. This classification is consistent with the swimming patterns observed in our numerical simulations (Fig. 3 and Supplementary Video S1). The results indicate that the differences in the net force and net torque directions acting on the cell body from the two flagellar apparatuses explain the mechanism by which the MO-1 cell model exhibits different swimming trajectories.

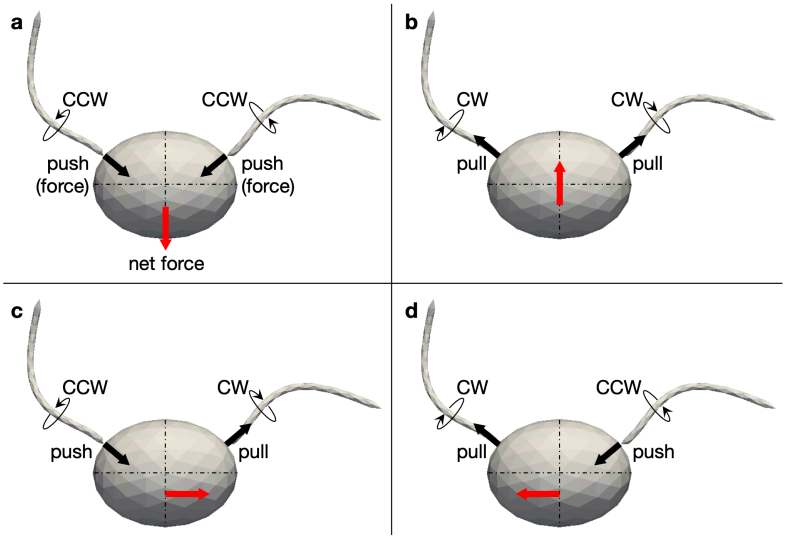

Fig. 4 Possible patterns of the approximated direction of net force from the flagella to cell body.

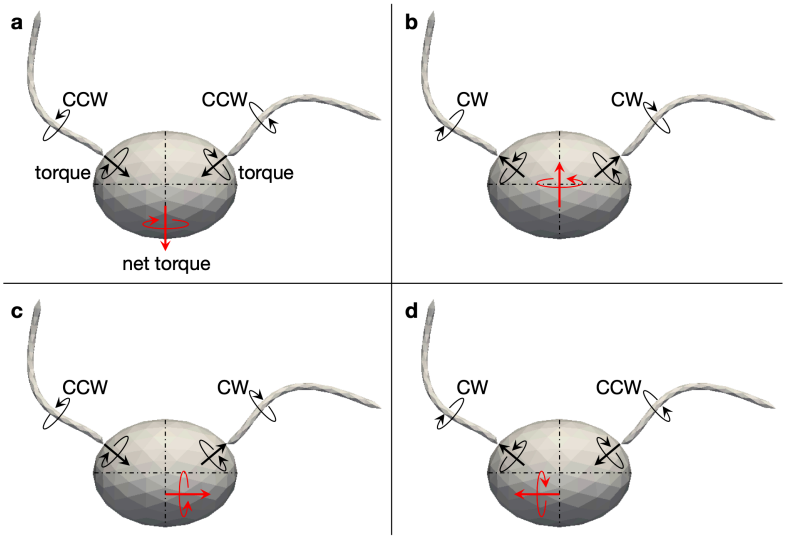

Fig. 5 Possible patterns of the approximated direction of net torque from the flagella to cell body.

[DOI: 10.1299/jbse.24-00284]

3.2 MO-1 cells swimming in helical trajectories

As shown in Fig. 3 and Supplementary Video S1, only a few combinations of flagellar helix chirality and rotary direction reproduced the helical trajectories of actual MO-1 cells (Fig. 2a, top). We verified the swimming motion of cell model ID4 because the cell models of ID8, ID12, and ID16 are equivalent to ID4 due to the geometric symmetry of flagellar helix chirality and rotary direction. In cell model ID4, flagellum 1 pulled the cell body, whereas flagellum 2 pushed it. The motion of the two flagellar apparatuses resulted in a helical trajectory. The pitch and diameter of the helical trajectory were 1.45 and 1.25 μm, respectively, under the cell body polar radius a = 1 μm. The ratio of the translational speed to the revolution rate was 1.48 μm. The cell body completed one rotation for each helical motion. We observed subtle vibrations in the trajectory, likely originating from the motion of the flagellar apparatuses, but we do not discuss these in the present paper.

Since our numerical simulations were performed using nondimensionalized physical quantities, it was necessary to assume the rotational speed of the flagellar apparatus in order to determine specific values for the translational speed and revolution rate. Therefore, we estimated the rotational speed of the flagellar apparatus in active MO-1 by using the rotation ratio (the number of flagellar rotations per revolution of the helical motion of the cell body) obtained from the numerical simulations and the revolution rate obtained from the experiments. In cell model ID4, the flagellar apparatus rotated 12 times per revolution of the helical motion of the cell body. The revolution rate of the actual MO-1 cells was approximately 100 s^{-1} (Fig. 2c). Thus, we estimated that the rotational speed of the flagellar apparatus in active MO-1 cells was approximately 1200 s^{-1}. The validity of this value will be discussed in Chapter 4. This is the fitting parameter introduced in this study. As shown in Fig. 2c, we determined the translational speed and revolution rate from the simulation results under the assumptions of the cell body polar radius a = 1 μm and the flagellar rotational speed f = 1200 s^{-1}.

To verify the simulation results, we compared them with experimental observations. Fig. 2b and c compare the diameter, pitch, translational speed, and revolution rate of the helical swimming trajectory in ID4 with those measured in experiments. In Fig. 2b and c, θ is the angle between the long axis of the cell body and the line connecting the cell center to each flagellar base (see Fig. 1b). The plots and error bars in Fig. 2b and c represent the means and standard deviations of simulation results under four different rotational phase differences (0°, 90°, 180°, and 270°) between the two flagellar apparatuses. The experimental and simulation results showed good agreement for both Fig. 2b (diameter versus pitch) and Fig. 2c (translational speed versus revolution rate). Thus, our cell model ID4 (and ID8, ID12, and ID16) is a valid model of the flagellar behavior in a swimming MO-1 cell.

3.3 MO-1 cell-specific swimming near a wall and its biological advantages

Many bacteria, such as *E. coli*, have been observed swimming along glass surfaces under a microscope. We investigated how a wall affects the helical swimming motion of our cell model. Conventional methods encounter technical difficulties in calculating the mechanical effects of walls (Bente et al., 2020). To clarify the advantage of the MO-1 cell, we compared the following four cases:

- case (a), which is equivalent to ID4;
- case (b), which has the same cell body shape and flagellar shape as ID4, but flagellum 1 does not rotate;
- case (c), which has the same cell body and flagellum 2 as ID4, but lacks flagellum 1; and
- case (d), which is an *E. coli* cell model with a single flagellum (Giacché et al., 2010).

Figure 6 shows the swimming trajectories of these four models near a wall at z = 0. The MO-1 cell model in case (a) swam away from the wall, and its trajectory viewed from the z-direction remained straight, even near the wall. This behavior significantly differed from the *E. coli* model with a single flagellum in case (d), which became bound to the wall and swam in a circular trajectory near it. Similar to case (d), the models of cases (b) and (c) also exhibited circular trajectories near the wall. The model of case (b) became bound to the wall, whereas the model of case (c) gradually swam away from it. In summary, only the MO-1 cell model of case (a) exhibited a straight trajectory in the x-y projection, even in the presence of a wall at z = 0, and it swam away from the wall.

In general, the cell body and flagellum of a swimming bacterium with a single rotating flagellum, such as in cases (b), (c), and (d), experience opposite drag forces from the wall due to their opposite rotary directions. These two opposite forces generate a wall-induced rolling torque in the z-direction, causing the trajectories in cases (b), (c), and (d) to roll near the wall. In contrast, the MO-1 cell model of case (a) experienced no wall-induced rolling torque because its two flagella had the same shape and opposite rotary directions, resulting in cancellation of the rolling torques caused by the

[DOI: 10.1299/jbse.24-00284]

two flagella. This explains why the MO-1 cell model in case (a) maintained the same motion as in solution without its trajectory bending due to the wall. To swim in a specific direction, MO-1 required the rotation of both flagellar apparatuses, rather than one apparatus alone.

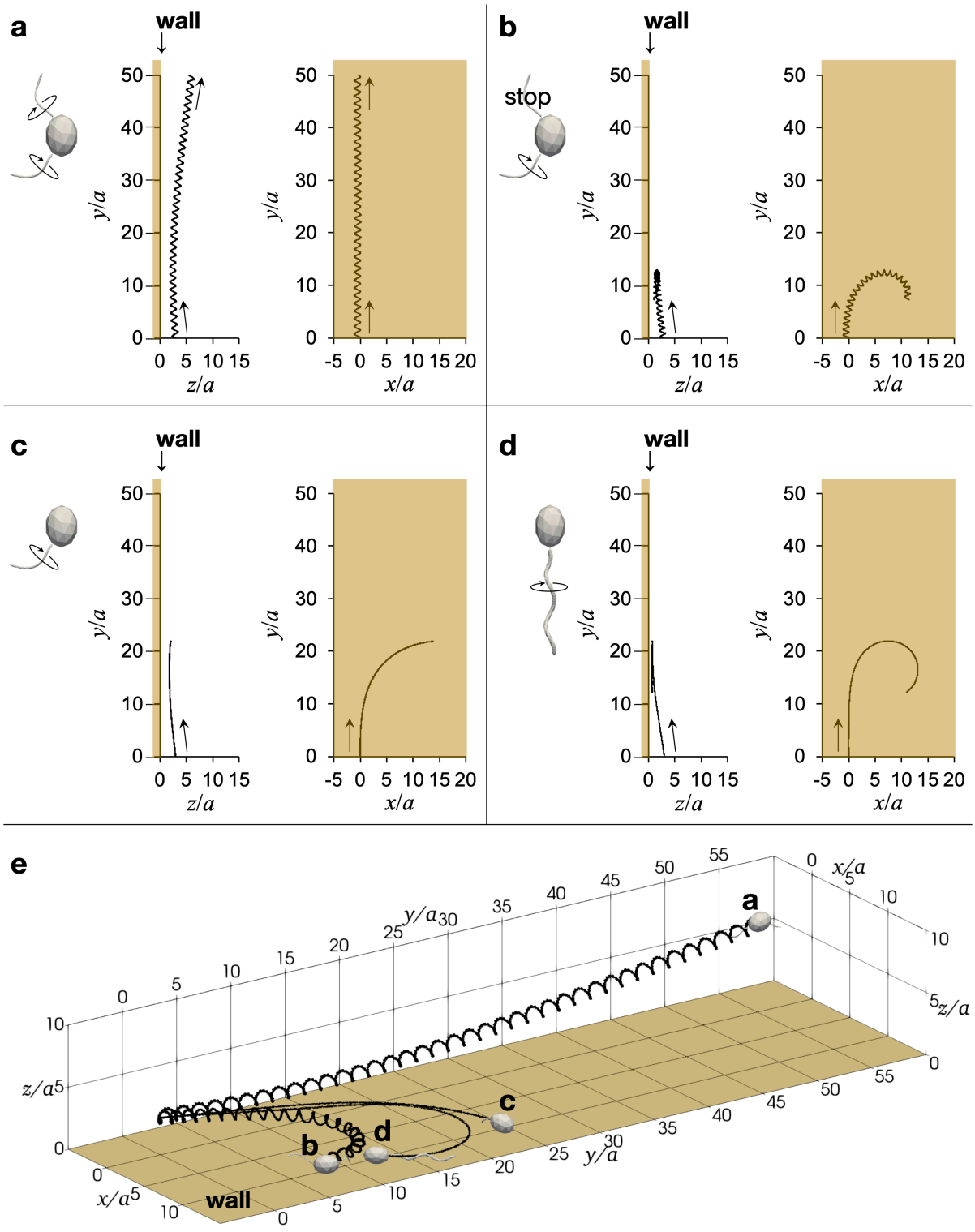

Fig. 6 Swimming trajectories of cell models near a wall at $z = 0$. (a) MO-1 cell model of ID4. (b) Cell model with the same cell body shape and flagellar shape as ID4, but flagellum 1 does not rotate. (c) Cell model with the same cell body and flagellum 2 as ID4, but without flagellum 1. (d) *E. coli* cell model with a single flagellum. (e) Isometric view showing all cases (a)-(d).

[DOI: 10.1299/jbse.24-00284]

4. Discussion

We constructed cell models that successfully reproduced the helical trajectories of actual MO-1 cells (Fig. 3 and Supplementary Video S1). The characteristic swimming motion resulted from the cell body being pulled by one flagellar apparatus in the front and pushed by another in the back, consistent with previous work (Bente et al., 2020). The helical swimming motion of the cell model showed good quantitative agreement with that of actual MO-1 cells (Fig. 2b and c).

We estimated the rotational speed of the flagellar apparatus in active MO-1 cells. By comparison with experimental results, we calculated the rotational speed to be approximately 1200 s^{-1}. This speed is about 4-fold higher than that of *E. coli* cells (~270 s^{-1}) (Kudo et al., 1990); however, it is comparable to that of the sodium-driven flagellar motor in *E. coli* (890 s^{-1}) (Sowa et al., 2010) and the polar flagellum in *Vibrio alginolyticus* cells (500~1700 s^{-1}) (Magariyama et al., 1995). These findings indicate that MO-1 cells utilize one of the fastest rotating machineries among bacterial flagellar apparatuses.

Finally, we discuss the biological advantages of the helical swimming motion of MO-1 cells. Magnetotactic bacteria contain magnetosomes (Bazylinski and Frankel, 2004; Zhang and Wu, 2020; Taoka et al., 2023), which orient them in the direction of magnetic field lines due to magnetic torque. Consequently, magnetotactic bacteria swim along magnetic field lines, a property called magnetotaxis. Earth's magnetic field lines are parallel to the surface at the equator, but the vertical component increases with latitude. Magnetotactic bacteria preferentially swim northward along magnetic field lines in the northern hemisphere (Blakemore, 1975) and southward in the southern hemisphere (Blakemore et al., 1980). Thus, in both hemispheres, magnetotactic bacteria swim toward the seafloor. Magnetotaxis is advantageous for magnetotactic bacteria that prefer the hypoxic environment of the seafloor. However, unlike near the sea surface, there are many sediments at depth. This means bacteria swim near walls much larger than their bodies. MO-1 cells near a wall maintain the same helical swimming motion as in solution without trajectory bending due to the wall. This ability is beneficial in situations where MO-1 cells move toward more suitable environments in the presence of many sediments. Our cell models demonstrate that MO-1 cells utilize two flagellar apparatuses, rather than one, for directional swimming.

5. Conclusion

We investigated the swimming motility of the magnetotactic bacterium MO-1 through numerical simulations based on the boundary element method. Only a few combinations of flagellar helix chirality and rotary direction reproduced the helical trajectories of actual MO-1 cells. We provided a physical explanation for this mechanism. We also observed MO-1 cells, and the observational and simulation results showed good quantitative agreement. Our estimation of the rotational speed of two flagellar apparatuses in active MO-1 cells suggests that MO-1 cells utilize one of the fastest rotating machineries among bacterial flagellar apparatuses. We also investigated the biological advantages of MO-1 cell-specific swimming near a wall. This investigation revealed why MO-1 uses two flagellar apparatuses, rather than one, for directional swimming.

Acknowledgments

We thank Dr. Tohru Minamino, Mr. Riku Enomoto, Mr. Taisei Nishiyama, and Mr. Sota Hasumi for valuable discussions. This work was funded by grants from the Japan Society for the Promotion of Science (JSPS KAKENHI Grant Numbers JP24K07308 to Y.S.; JP24117004 and JP16K14682 to T.K.; 21H04999 and 21H05308 to T.I.; JP25000013 to K.N.; JP15H01319, JP22H05697 and JP23K23190 to M.N.), by Platform Project for Supporting Drug Discovery and Life Science Research (BINDS) from AMED under Grant Number JP18am0101117 to K.N. and by JEOL YOKOGUSHI Research Alliance Laboratories of Osaka University to K.N.

Conflict of interest

There are no conflicts of interest.

[DOI: 10.1299/jbse.24-00284]

References

Armitage, J. P., Twists and turns: 40 years of investigating how and why bacteria swim, Microbiology, Vol. 170, No. 2 (2024), 001432, DOI: 10.1099/mic.0.001432.

Bazylinski, D. A. and Frankel R. B., Magnetosome formation in prokaryotes, Nature Review Microbiology, Vol. 2, No. 3 (2004), pp. 217-230, DOI: 10.1038/nrmicro842.

Bente, K., Mohammadinejad, S., Charsooghi, M. A., Bachmann, F., Codutti, A., Lefèvre, C. T., Klumpp, S. and Faivre, D., High-speed motility originates from cooperatively pushing and pulling flagella bundles in bilophotrichous bacteria, eLife, Vol. 9 (2020), e47551, DOI: 10.7554/eLife.47551.

Berg, H. C., The rotary motor of bacterial flagella, Annual Review of Biochemistry, Vol. 72 (2003), pp. 19-54, DOI: 10.1146/annurev.biochem.72.121801.161737.

Blakemore, R., Magnetotactic bacteria, Science, Vol. 190, No. 4212 (1975), pp. 377-379, DOI: 10.1126/science.170679.

Blakemore, R., Frankel, R. and Kalmijn, A., South-seeking magnetotactic bacteria in the Southern Hemisphere, Nature, Vol. 286 (1980), pp. 384-385, DOI: 10.1038/286384a0.

Giacché, D., Ishikawa, T. and Yamaguchi, T., Hydrodynamic entrapment of bacteria swimming near a solid surface, Physical Review E, Vol. 82 (2010), 056309, DOI: 10.1103/PhysRevE.82.056309.

Higdon, J. J. L., The hydrodynamics of flagellar propulsion: helical waves, Journal of Fluid Mechanics, Vol. 94, No. 2 (1979), pp. 331-351, DOI: 10.1017/S0022112079001051.

Homma, M. and Kojima, S., The Periplasmic Domain of the Ion-Conducting Stator of Bacterial Flagella Regulates Force Generation, Frontiers in Microbiology, Vol. 13 (2022), 869187, DOI: 10.3389/fmicb.2022.869187.

Ishikawa, T., Sekiya, G., Imai, Y. and Yamaguchi, T., Hydrodynamic interactions between two swimming bacteria, Biophysical Journal, Vol. 93, No. 6 (2007), pp. 2217-2225, DOI: 10.1529/biophysj.107.110254.

Ji, B., Zhang, S. D., Zhang, W. J., Rouy, Z., Alberto, F., Santini, C. L., Mangenot, S., Gagnot, S., Philippe, N., Pradel, N., Zhang, L., Tempel, S., Li, Y., Médigue, C., Henrissat, B., Coutinho, P. M., Barbe, V., Talla, E. and Wu, L. F., The chimeric nature of the genomes of marine magnetotactic coccoid-ovoid bacteria defines a novel group of Proteobacteria, Environmental Microbiology, Vol. 19, No.3 (2017), pp. 1103-1119, DOI: 10.1111/1462-2920.13637.

Kogure, Y., Omori, T. and Ishikawa, T., Flow-induced diffusion in a packed lattice of squirmers, Journal of Fluid Mechanics, Vol. 971 (2023), A17, DOI: 10.1017/jfm.2023.651.

Kudo, S., Magariyama, Y. and Aizawa, S., Abrupt changes in flagellar rotation observed by laser dark-field microscopy, Nature, Vol. 346, No. 6285 (1990), pp. 677-680, DOI: 10.1038/346677a0.

Lefèvre, C. T., Bernadac, A., Yu-Zhang, K., Pradel, N. and Wu, L. F., Isolation and characterization of a magnetotactic bacterial culture from the Mediterranean Sea, Environmental Microbiology, Vol. 11, No. 7 (2009), pp. 1646-1657, DOI: 10.1111/j.1462-2920.2009.01887.x.

Lefèvre, C. T., Santini, C. L., Bernadac, A., Zhang, W. J., Li, Y. and Wu, L. F., Calcium ion-mediated assembly and function of glycosylated flagellar sheath of marine magnetotactic bacterium, Molecular Microbiology, Vol. 78, No. 5 (2010), pp. 1304-1312, DOI: 10.1111/j.1365-2958.2010.07404.x.

Magariyama, Y., Sugiyama, S., Muramoto, K., Kawagishi, I., Imae, Y. and Kudo, S., Simultaneous measurement of bacterial flagellar rotation rate and swimming speed, Biophysical Journal, Vol. 69, No. 5 (1995), pp. 2154-2162, DOI: 10.1016/S0006-3495(95)80089-5.

Minamino, T. and Kinoshita, M., Structure, Assembly, and Function of Flagella Responsible for Bacterial Locomotion, EcoSal Plus, Vol. 11, No. 1 (2023), eesp00112023, DOI: 10.1128/ecosalplus.esp-0011-2023.

Miyata, M., Robinson, R. C., Uyeda, T. Q. P., Fukumori, Y., Fukushima, S. I., Haruta, S., Homma, M., Inaba, K., Ito, M., Kaito, C., Kato, K., Kenri, T., Kinosita, Y., Kojima, S., Minamino, T., Mori, H., Nakamura, S., Nakane, D., Nakayama, K., Nishiyama, M., Shibata, S., Shimabukuro, K., Tamakoshi, M., Taoka, A., Tashiro, Y., Tulum, I., Wada, H. and Wakabayashi, K. I., Tree of motility - A proposed history of motility systems in the tree of life, Genes to Cells, Vol. 25, No. 1 (2020), pp. 6-21, DOI: 10.1111/gtc.12737.

Nishiyama, M. and Sowa, Y., Microscopic analysis of bacterial motility at high pressure, Biophysical Journal, Vol. 102, No. 8 (2012), pp. 1872-1880, DOI: 10.1016/j.bpj.2012.03.033.

Okuno, D., Nishiyama, M. and Noji, H., Single-molecule analysis of the rotation of F_1-ATPase under high hydrostatic pressure, Biophysical Journal, Vol. 105, No. 7 (2013), pp. 1635-1642, DOI: 10.1016/j.bpj.2013.08.036.

Ruan, J., Kato, T., Santini, C. L., Miyata, T., Kawamoto, A., Zhang, W. J., Bernadac, A., Wu, L. F. and Namba, K., Architecture of a flagellar apparatus in the fast-swimming magnetotactic bacterium MO-1, Proceedings of the National Academy of Sciences of the United States of America, Vol. 109, No. 50 (2012), pp. 20643-20648, DOI: 10.1073/pnas.1215274109.

Shimogonya, Y., Sawano, Y., Wakebe, H., Inoue, Y., Ishijima, A. and Ishikawa, T., Torque-induced precession of bacterial flagella, Scientific Reports, Vol. 5 (2015), 18488, DOI: 10.1038/srep18488.

Shum, H., Gaffney, E. A. and Smith, D. J., Modelling bacterial behaviour close to a no-slip plane boundary: the influence of bacterial geometry, Proceedings of the Royal Society A, Vol. 466 (2010), pp. 1725-1748, DOI: 10.1098/rspa.2009.0520.

Sowa, Y., Steel, B. C. and Berry, R. M., A simple backscattering microscope for fast tracking of biological molecules, Review of Scientific Instruments, Vol. 81, No. 11 (2010), 113704, DOI: 10.1063/1.3495960.

Taoka, A., Eguchi, Y., Shimoshige, R. and Fukumori, Y., Recent advances in studies on magnetosome-associated proteins composing the bacterial geomagnetic sensor organelle, Microbiology and Immunology, Vol. 67, No. 5 (2023), pp. 228-238, DOI: 10.1111/1348-0421.13062.

Yang, C., Chen, C., Ma, Q., Wu, L. and Song, T., Dynamic Model and Motion Mechanism of Magnetotactic Bacteria with Two Lateral Flagellar Bundles, Journal of Bionic Engineering, Vol. 9, No. 2 (2012), pp. 200-210, DOI: 10.1016/S1672-6529(11)60108-X.

Yang, J., Shimogonya, Y. and Ishikawa, T., Bacterial detachment from a wall with a bump line, Physical Review E, Vol. 99 (2019), 023104, DOI: 10.1103/PhysRevE.99.023104.

Youngren, G. K. and Acrivos, A., Stokes flow past a particle of arbitrary shape: a numerical method of solution, Journal of Fluid Mechanics, Vol. 69, No. 2 (1975), pp. 377-403, DOI: 10.1017/S0022112075001486.

Zhang, S. D., Petersen, N., Zhang, W. J., Cargou, S., Ruan, J., Murat, D., Santini, C. L., Song, T., Kato, T., Notareschi, P., Li, Y., Namba, K., Gué, A. M. and Wu, L. F., Swimming behaviour and magnetotaxis function of the marine bacterium strain MO-1, Environmental Microbiology Reports, Vol. 6, No. 1 (2014), pp.14-20, DOI: 10.1111/1758-2229.12102.

Zhang, W. J., Santini, C. L., Bernadac, A., Ruan, J., Zhang, S. D., Kato, T., Li, Y., Namba, K. and Wu, L. F., Complex spatial organization and flagellin composition of flagellar propeller from marine magnetotactic ovoid strain MO-1, Journal of Molecular Biology, Vol. 416, No. 4 (2012), pp. 558-570, DOI: 10.1016/j.jmb.2011.12.065.

Zhang, W. J. and Wu, L. F., Flagella and Swimming Behavior of Marine Magnetotactic Bacteria, Biomolecules, Vol. 10, No. 3 (2020), 460, DOI: 10.3390/biom10030460.

[DOI: 10.1299/jbse.24-00284]